Optics & Laser Technology 41 (2009) 310–317

Contents lists available at ScienceDirect

Optics & Laser Technology

journal homepage: www.elsevier.com/locate/optlastec

A novel video opto-mechanical (VOM) device for studying the effect of stretching speed on the optical and structural properties of fibers

T.Z.N. Sokkar [a], M.M. El-Tonsy [a], M.A. El-Bakary [a], M.A. El-Morsy [b], A.M. Ali [a,*]

[a] Physics Department, Faculty of Science, Mansoura University, Mansoura 35516, Egypt
[b] Physics Department, Demietta Faculty of Science, Mansoura University, New Demietta, Egypt

ARTICLE INFO

Article history:
Received 6 February 2008
Received in revised form
20 May 2008
Accepted 30 May 2008
Available online 9 July 2008

Keywords:
Stretching
Dynamic
Refractive index

ABSTRACT

Using a novel video opto-mechanical (VOM) device, the effect of stretching speed on the optical and structural properties of polypropylene (PP) fibers during the dynamic stretching process is studied. The objective of the present study is to correlate the optical and mechanical properties of PP fibers with the speed of stretching using the multiple-beam Fizeau fringes system. The skeletonization of the multiple-beam Fizeau fringes are determined automatically by using one-dimension Fourier transform method. The stepper motor is adjusted in order to stretch the fibers continuously with constant and uniform speed until breaking of the fiber. The refractive indices, birefringence, transverse sectional area and the orientation function of PP fibers are studied as a function of the draw ratio at different speeds of stretching. An empirical formula is given to correlate the birefringence of PP fiber and both the draw ratio and the speed of stretching. Stretching process of PP with low speed (slow stretching) is recommended to overcome the necking deformation along the fiber. The VOM device could be used to measure the yield strain. The draw ratio-stretching speed superposition is discussed with some details. Microinterferograms are given for illustration.

1. Introduction

Polypropylene (PP) is extensively used in industry to manufacture bottles, films and fibers. The heat and draw deformation behavior of PP is of significant practical importance in terms of both its product performances and manufacturing processes. The mechanical properties and morphology of the product are strongly affected not only by its molecular characteristics such as the molecular weight (MW), molecular weight distribution (MWD) [1,2], but also by its processing conditions such as drawing temperature, the draw ratio, the strain rate and the cooling after stretching. Therefore, understanding the structural deformation behavior during processing is essential for the quantitative predictions of improved product performance and the stretching tension [3,4].

The increased applications of polymers and their composites for light-weight structures has led to renewed interest in the study of deformation behavior at different loading rates and impact conditions [5–7]. The primary objective of understanding the deformation behavior at varying strain rates is to assist the designer with reliable data relevant to practical applications. The study of deformation behavior at different strain rates is important in engineering design because the mechanical properties and the deformation mechanisms are strongly dependent on the applied strain rate.

Stretching of the fiber concerns the deformation of the pre-existing structure of this fiber. In the stretching process, changes in the optical properties have been determined by the interferometric methods [8–10]. Thus, the influence of the draw ratio upon the structure changes occurring in the synthetic fibers is also indicated. Molecules are oriented parallel to the fiber axis, and the stretching may produce a fringed fibril structure with the molecules lying parallel to the axis of the crystalline fiber. The initial effect of the fibrils is thus by increasing the transverse orientation of the molecules. If the stretching is continued, this will be followed by a change to longitudinal orientation of the molecules [11,12].

The multiple-beam Fizeau interferometric system is a sensitive optical technique. This interferometric method improved greatly and became more efficient with the introduction of automated methods of image analysis, so the multiple-beam Fizeau fringe systems in transmission (cf. Refs. [13,14]) were modified by adding a CCD camera and frame grabber digitizer to transfer the image into an image analysis screen to be analyzed automatically. The resulting fringes give qualitative and quantitative information about the optical and structural properties of the fibers under investigation. Multiple-beam interferometric technique has been used to determine the refractive index,

* Corresponding author. Tel.: +20 50 236 1852.
E-mail address: afaf12004@yahoo.com (A.M. Ali).

0030-3992/$ - see front matter © 2008 Elsevier Ltd. All rights reserved.
doi:10.1016/j.optlastec.2008.05.027

birefringence and dispersion of man-made fibers. The automated and high-speed image processing system is used to analyze the fringe pattern and gives an accurate analysis. The principle method in automatic fringe-pattern analysis is fringe skeleton extraction [15].

In this article, a novel video opto-mechanical (VOM) device is designed to be used for the mechanical stretching of fibers. The material is an isotactic PP was received as a commercial sample entitled "As spun/undrawn PP fibers. The VOM device attached with multiple-beam interference system to correlate the optical, mechanical and structural properties of fibers with the speed of stretching. The refractive indices, birefringence and the transverse sectional area and orientation function of PP fibers will be studied as a function of draw ratio at different stretching speed. Also, the draw ratio-stretching speed superposition will be discussed with some details.

2. Setup of VOM device and experimental technique

A VOM is designed in order to determine dynamically the mechanical, optical and structural properties of fibers with different uniform stretching speeds and also to determine properties of fibers during online stretching until the breaking. The VOM device attached with multiple-beam interferometric system is an accurate and an efficient technique in the field of interferometery and monitoring (mechanical properties) of fibers. This VOM setup used in this work consists of three units (see Fig. 1);

2.1. Interferometric unit

"Fizeau interferometric system in transmission (cf. Refs. [13,14])". This optical system produces multiple-beam Fizeau fringes in transmission. This system (see Fig. 1(a)) consists of, a spectral lamp (1), condenser (2), iris diaphragm (3), collimating lens (4), polarizer (5), monochromatic filter (6), reflector (7), microscope stage (8) and liquid wedge interferometer (14).

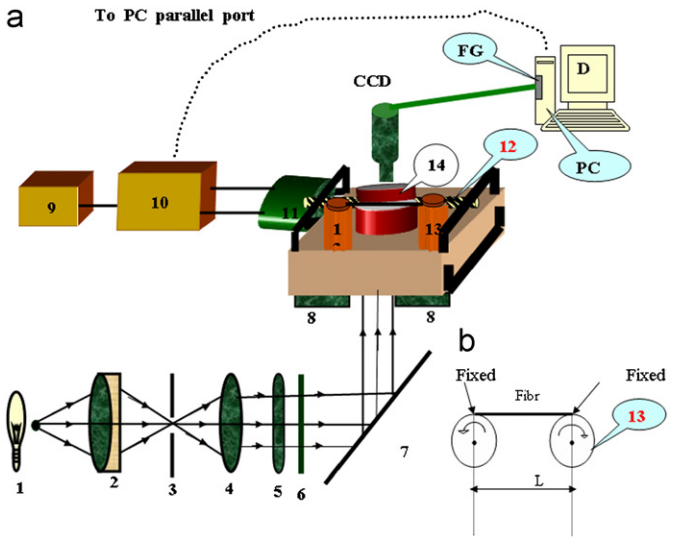

Fig. 1. (a) A schematic diagram of the optical and the mechanical setup of video opto-mechanical (VOM), in which; 1—spectrum lamp, 2—condenser lens, 3—iris diaphragm, 4—collimating lens, 5—polarizer, 6—monochromatic filter, 7—reflector, 8—microscope stage, 9—DC battery, 10—stepper motor interface, 11—stepper motor, 12—bidirectional driving axis, 13—two gear box, 14—silvered liquid wedge interferometer, 15—computer unit (b) Gear box rotating wheels.

2.2. Mechanical unit

The unit consists of a DC battery (9), stepper motor interface (10) to transfer the digital pulse from the computer to the four pin and 48 step/360° stepper motor (11), which forces the bidirectional axis to move with definite speed, the bidirectional driving axis (12), which forces the two gear boxes (13), to move in opposite directions (with rotational reduction factor (1/28)) to stretch the fiber. Where 28 is the number of the gear box steps. In order to pre-calculate the stretching ratio DR in terms of motor speed, it is essential to define the machine constant M (stretching resolution of the machine) of this device as the linear displacement of the fiber fixed end per step of the used stepper motor. The motor in Fig. 1(b) makes 48 step/revolution, hence

$$M = (2\pi r) \times \left(\frac{1}{28}\right) \times \left(\frac{1}{48}\right) \text{ cm/step} \tag{1}$$

where r is the radius of the gear box rotating from wheel. The draw ratio (DR) ranged from 1 to 12 and also the speed (V) 0.0596 to 12 cm/s. Then the elongation rate Δl (Δl may be used as the stretching speed (V) in cm/s) is

$$\Delta l = 2Mf = V \text{ cm/s} \tag{2}$$

where f is the frequency of rotation in step/s, the factor 2 refers to stretching the fiber by two similar wheels in opposite directions simultaneously, and hence the net elongation ΔL of the fiber during time interval t is

$$\Delta L = \Delta l t = 2Mft \tag{3}$$

Thus, it is possible to stretch the fiber to a definite elongation ΔL at a definite speed (Δl) by careful (software) selection of both f and t.

Accordingly, the draw ratio DR that defined as

$$\text{DR} = \frac{\Delta L}{L} + 1 \tag{4}$$

where L is the initial (undrawn) length of the fiber sample (normally, L = distance separating centers of gear box rotating wheels, Fig. 1(b)), then

$$\text{DR} = \frac{2M}{L} ft + 1 \tag{5}$$

and the strain rate can be estimated from the relation:

$$\text{strain rate} = \frac{\Delta l}{L} = \frac{2Mf}{L} \tag{6}$$

2.3. Computerized unit

This unit consists of a panasonic CCD micro-camera, PC computer, digital frame grabber memory (FG) and digital monitor (DM).

This experimental setup (Fig. 1) is used for determining the refractive index during the online stretching of PP fibers as follows; firstly, on the lower optical flat of the liquid wedge interferometer (14), a sample of certain length from PP fibers is linked from its ends with the gear box of the stretching system (13). Few drops of an immersion liquid having refractive index close to that of the fiber are put on the fixed fiber on the lower optical flat of the interferometer and then the mechanical system is transferred to the optical interference system. A parallel beam of polarized monochromatic light is incident perpendicular to the liquid wedge interferometer, which is adjusted in such a way that the fiber axis is exactly perpendicular to the interference fringes in the liquid region.

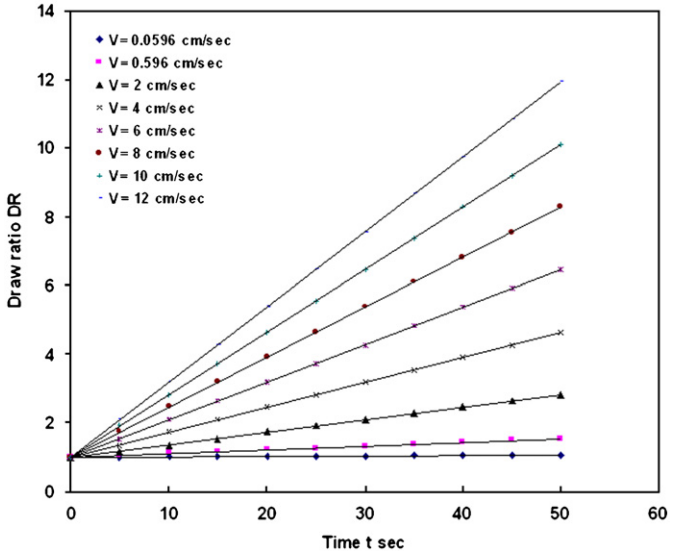

Fig. 2. The calibration curve of the device (shows the variation of the draw ratio with the time of stretching at different stretching speed).

The stepper motor speed is adjusted by taking a definite number of steps using a software programme installed in the computer system. The CCD camera is adjusted to capture the output image from the microscope life without stopping until the fiber breaking region is reached. Also the CCD camera is adjusted to capture 25 frames/s during the stretching process of PP fibers. The obtained fiber video film is recorded using the CCD camera and the computerized unit. This film is digitized directly via the digitizer frame grabber. The video film is cut into separate frames. These images are enhanced and the noise is removed by using Fourier transform method. The obtained contour lines are analyzed via a software program for fiber refractive index determination [15].

The designed (VOM) device is calibrated in order to determine the draw ratio of the fiber directly from the recorded video film. Fig. 2 shows the calibration curve of the device (the variation of the draw ratio with the time of stretching at different stretching speed). The following empirical equation expresses the relation between the draw ratio and the time of stretching:

$$\mathrm{DR} = 0.1172Vt + 1 \tag{7}$$

where DR is the draw ratio, V is the speed of the stepper motor and t is the time of chosen frame from the video film recorded. Where the constant (0.1172) is the reciprocal of the fiber length (L).

3. Experimental results and discussion

3.1. Effect of the stretching speed on the birefringence of PP fibers

A PP fiber sample with a certain length is fixed from its ends with the two gear boxes (13) and mounted on the lower optical flat of the wedge interferometer (14). The fiber filament is immersed in a suitable liquid with refractive index $n_L = 1.5001$, close to the parallel refractive index of the fiber, at temperature ($T = 30\,^{\circ}\mathrm{C}$). The mechanical system is transferred to the optical microscope. The wavelength of monochromatic light used is 546.1 nm. The speed of stretching is adjusted to be 12 cm/s. The obtained video film is cut into separate images to deal with each frame individual. The draw ratio for each frame is calculated using Eq. (7). Fig. 3(a) shows some of the contour lines obtained

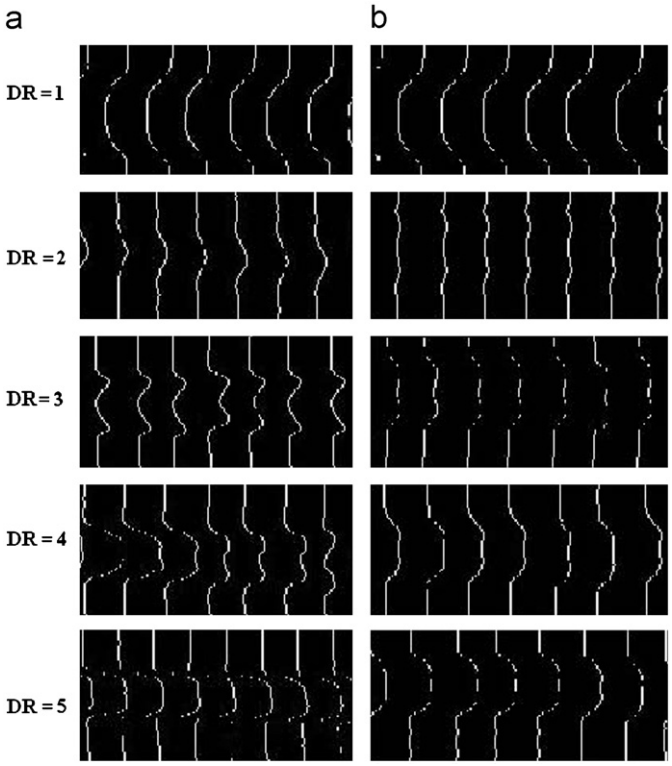

Fig. 3. (a and b) Some of the obtained contour lines of the multiple-beam Fizeau fringes microinterferograms of PP fibers at different draw ratios for light vibrating parallel to the fiber axis (a) $V = 12$ cm/s and (b) $V = 0.0596$ cm/s.

dynamically of the experimental microinterferograms of PP fibers at different draw ratios for light vibrating parallel to the fiber axis and speed equals to 12 cm/s.

Another filament of PP fiber is immersed in a liquid with refractive index $n_L = 1.492$ close to the perpendicular refractive index of the fiber, at temperature $T = 30\,^{\circ}\mathrm{C}$. The speed of stretching is adjusted to 12 cm/s. Fig. 4(a) shows some of the obtained contour lines of enhancement experimental microinterferograms of PP fibers at different draw ratios for light vibrating perpendicular to the fiber axis and the speed is $V = 12$ cm/s. The above steps are repeated at different stretching speed (0.0596–10 cm/s). Figs. 3(b) and 4(b) show the enhancement microinterferograms of PP fibers at different draw ratios for light vibrating parallel and perpendicular to the fiber axis, respectively, for the stretching speed $V = 0.0596$ cm/s. It is clear from Figs. 3(a) and 4(a), and 3(b) and 4(b) that there are great changes for the contour lines of fringe shifts at same draw ratio. This indicates that the speed of stretching affects the optical properties of fibers. The shape change of the fringe shift (shape of contour line) obtained in Figs. 3 and 4 is due to the deformation occurred in cross-section during the stretching process. This conclusion is supported by the reshaping of the fringe into elliptical one at higher draw ratio for the same sample. To determine these mean findings, the mean refractive indices ($n^{\parallel}$ and $n^{\perp}$) of PP fibers are calculated with the aid of the microinterferograms of Figs. 3 and 4 and using the following equation [14]:

$$n^j = n_L \pm \frac{F^j \lambda}{2bA} \tag{8}$$

where j denotes the state of light polarization parallel $\parallel$ or perpendicular $\perp$, n_L is the refractive index of the immersion liquid, F is the area enclosed under the fringe shift inside the fiber, λ is the wavelength of the monochromatic light used, b is the interfringe spacing, A is the fiber cross-sectional area and the

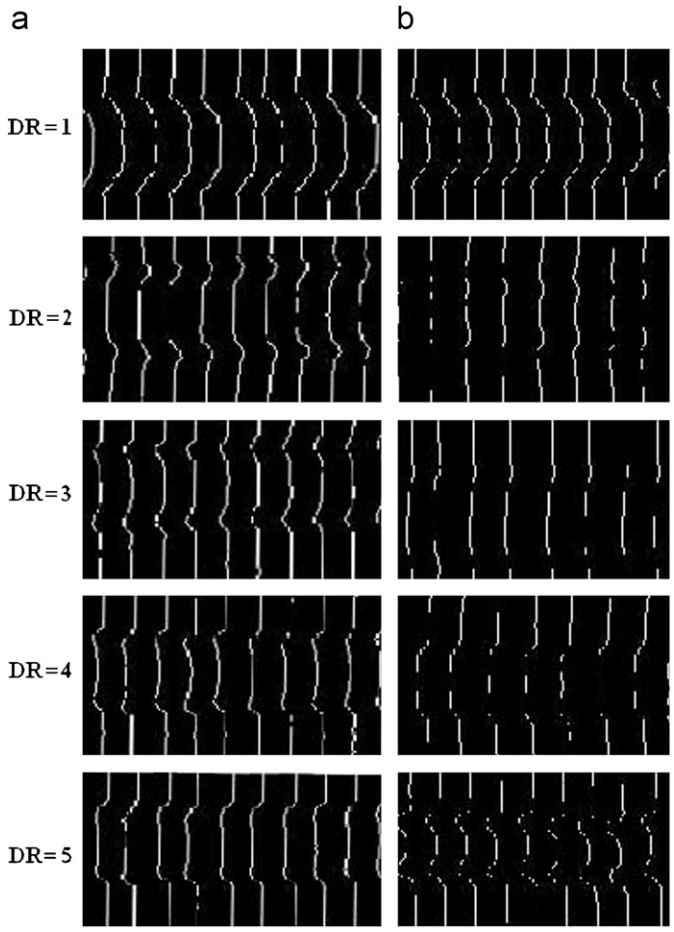

Fig. 4. (a and b) Some of the obtained contour lines of the multiple-beam Fizeau fringes microinterferograms of PP fibers at different draw ratios for light vibrating perpendicular to the fiber axis (a) $V = 12$ cm/s and (b) $V = 0.0596$ cm/s.

sign ($\pm$) depends on the direction of the fringe shift inside the fiber. A set of about eight samples were used to measure the average values of $n^{\parallel}$ and $n^{\perp}$ within the same range of draw ratio that followed in this work. Figs. 5(a) and 6(a) show the variation of the average refractive indices $n^{\parallel}$ and $n^{\perp}$ with the draw ratio, respectively, at different stretching speed. Figs. 5(b) and 6(b) show the variation of the average refractive indices with the stretching speed at different draw ratio. The birefringence of PP fibers is calculated from the measured refractive indices using the following equation:

$$\Delta n = n^{\parallel} - n^{\perp} \tag{9}$$

where $n^{\parallel}$ and $n^{\perp}$ are the parallel and the perpendicular refractive indices of the fiber, respectively. Fig. 7(a) shows the variation of the average birefringence of PP fibers with the draw ratio at different stretching speed. Fig. 7(b) shows the variation of the average birefringence of PP fibers with the stretching speed at different draw ratio.

It is clear from Fig. 5(a) that the value of average parallel refractive index increases with increasing the draw ratio. But those of the average perpendicular refractive index decrease with increasing the draw ratio as shown in Fig. 6(a). The increase of the refractive index $n^{\parallel}$ for light vibrating parallel to the fiber axis indicates that the molecules constituting the fiber are oriented or aligned in parallel direction more than the perpendicular one during the online stretching process. It was proposed that as an approximation, the polymer could be considered as aggregate units, which in the unstretched material are oriented randomly.

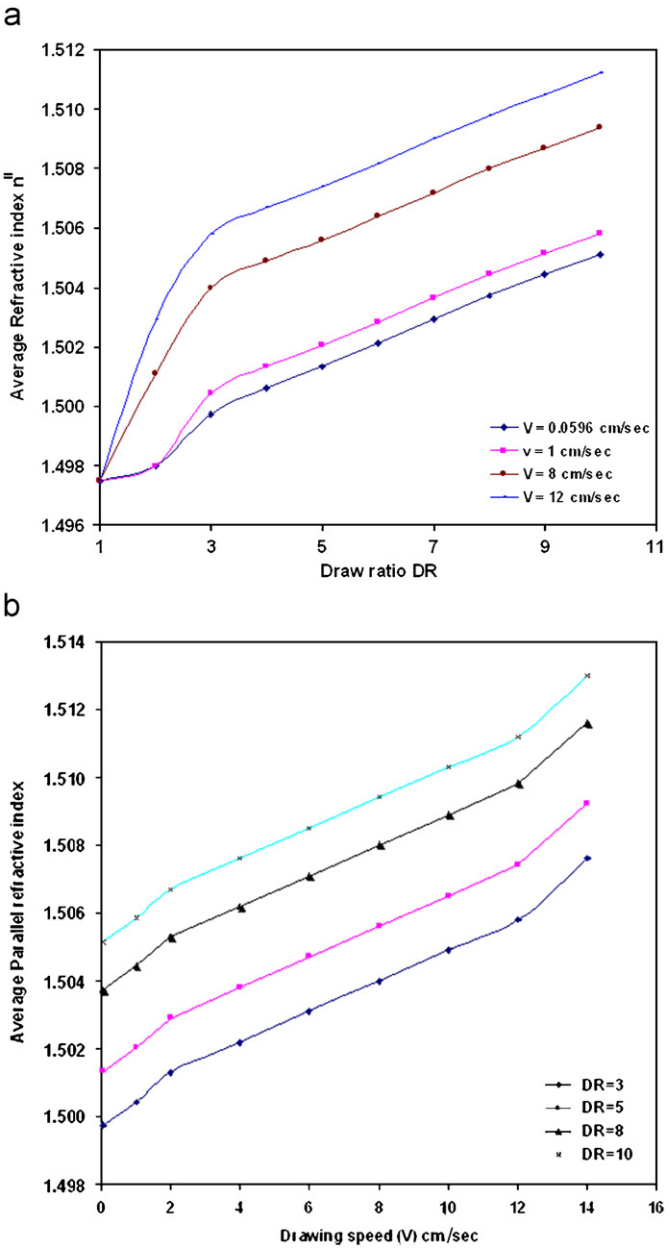

Fig. 5. Variation of the average refractive index $n^{\parallel}$ with the (a) draw ratio at different stretching speed. and (b) $n^{\parallel}$ with the stretching speed at different draw ratio.

As orientation develops by stretching, the units rotate towards the stretch direction and become completely aligned at the maximum achievable orientation [16]. As the speed of stretching increases the orientation process or the alignment of molecules toward the stretching direction increases and becomes the more occurring phenomena. So that the average parallel refractive index increases rapidly with increasing the stretching speed. From Figs. 5(b) and 7(b) it is clear that the parallel refractive index and the birefringence of PP fibers increase with increasing the speed of stretching for the same draw ratio, while the perpendicular refractive index decreases with increasing the speed of stretching of the same draw ratio (Fig. 6(b)). Figs. 5 and 6(a and b) indicate that the alignment of molecules or chains in the parallel direction is more than that of the perpendicular direction.

From Fig. 7(a) an empirical formula correlating the average birefringence (Δn), the speed (V) and the draw ratio DR is given

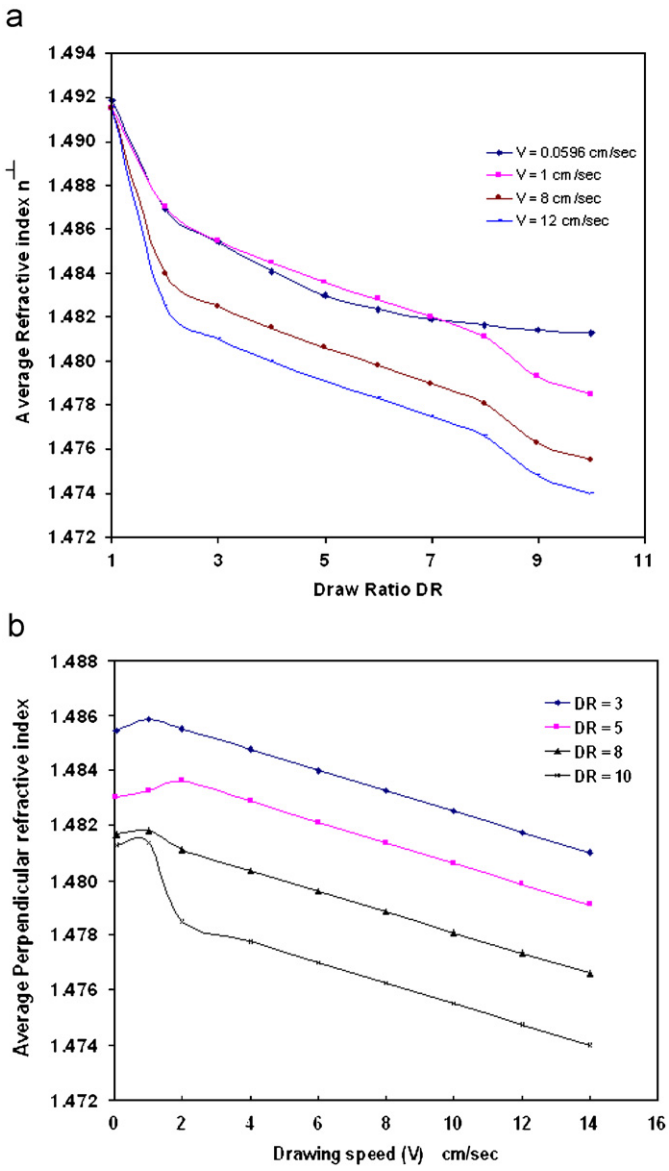

Fig. 6. Variation of the average refractive index $n^{\perp}$ (a) with the draw ratio at different stretching speed and (b) $n^{\perp}$ with the stretching speed at different draw ratio.

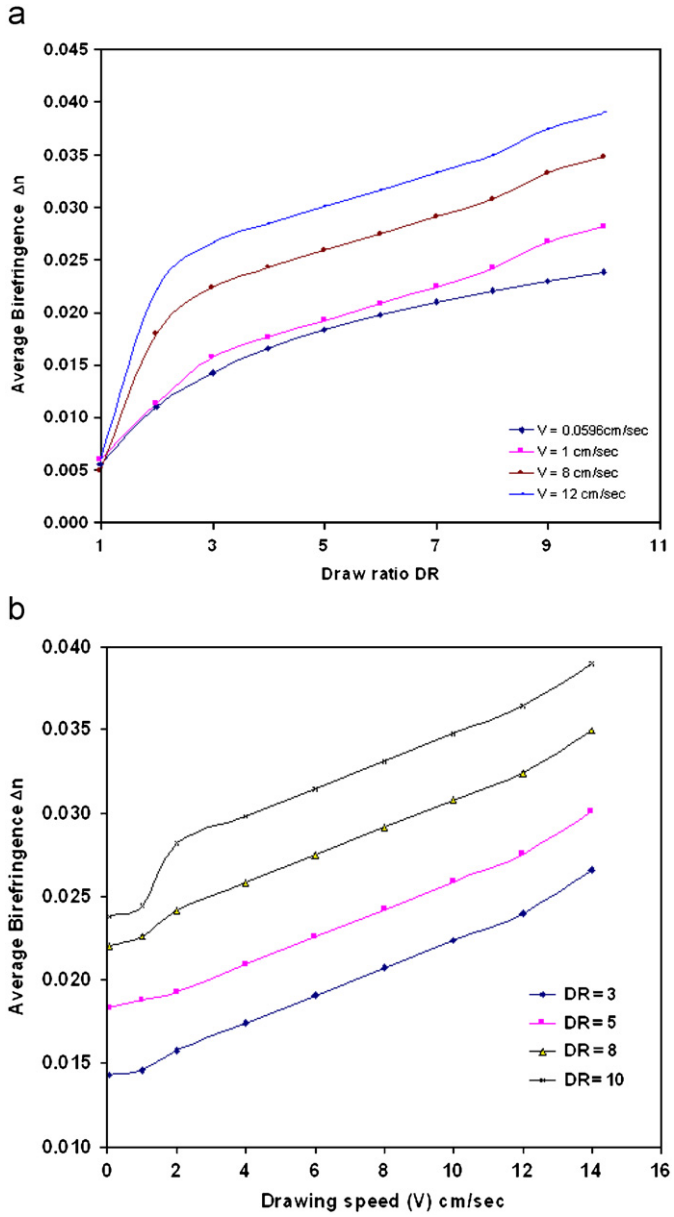

Fig. 7. Variation of the average birefringence of PP fibers (a) with the draw ratio at different stretching speed and (b) with the stretching speed at different draw ratio.

as follows:

$$\Delta n = \left(\frac{V}{V_0} + 0.0079\right) \ln(\mathrm{DR}) + \Delta n_0 \tag{10}$$

where DR is the draw ratio of the sample, and $\Delta n_0 = 0.0056$ (initial birefringence of the undrawn sample), V is the speed of stretching and $V_0 = 3333$ cm/s. It is a constant may be depending on the structural properties of PP fiber.

Eq. (10) is similar to the flowing empirical formula suggested by de Vrise [17]

$$\Delta n = m \ln(\mathrm{DR}) \tag{11}$$

de Vrise did not study the constant m. The present empirical formula shows that the constant m is a function of the stretching speed V. Eq. (10) can be rewritten as follows:

$$\Delta n = m(V) \ln(\mathrm{DR}) + \Delta n_0 \tag{12}$$

The suggested empirical formula may be used to predict the birefringence of drawn fiber with desired speed.

The error in measuring the speed (accuracy of designed device or stretching resolution of the machine) is ± 0.0149 cm/s. The accuracy in measuring the fringe shift that is produced by multiple-beam techniques are remarkably high because the interference fringes produced from these techniques are extremely sharp and the fringe displacement is proportional to twice the phase difference introduced by the fiber [14]. The error in the refractive index measurements is ± 0.0007 [18].

3.2. *Effect of stretching speed on the orientation function of PP fibers*

To confirm the effect of stretching speed on the structure of PP fibers, the orientation function is calculated. For a drawn fiber where the molecules are considered to be aligned along the draw direction but only randomly arranged in the transverse section, the optical properties of the system can be specified by only two refractive indices $n^{\parallel}$ parallel and $n^{\perp}$ perpendicular to the fiber axis.

Table 1
The variation of the orientation function with the draw ratio at different speeds

DR	$F(\theta)$ $V = 0.0596$ cm/s	$F(\theta)$ $V = 1$ cm/s	$F(\theta)$ $V = 2$ cm/s	$F(\theta)$ $V = 4$ cm/s	$F(\theta)$ $V = 6$ cm/s	$F(\theta)$ $V = 8$ cm/s	$F(\theta)$ $V = 10$ cm/s	$F(\theta)$ $V = 12$ cm/s
1	0.1244	0.124	0.124	0.124	0.124	0.124	0.124	0.124
2	0.246	0.250	0.253	0.290	0.326	0.363	0.400	0.436
3	0.317	0.324	0.351	0.387	0.424	0.461	0.497	**0.534**
4	0.368	0.377	0.393	0.430	0.466	0.503	0.540	0.576
5	0.407	0.417	0.428	0.465	0.502	0.538	0.575	0.612
6	0.439	0.450	0.464	0.501	0.537	0.574	0.611	0.647
7	0.466	0.479	0.500	0.536	0.573	0.610	0.646	0.683
8	0.490	0.503	0.537	0.574	0.611	0.647	0.684	0.721
9	0.511	0.524	0.593	0.630	0.666	0.703	0.740	0.776
10	**0.529**	0.544	0.626	0.663	0.700	0.736	0.773	0.810

The Herman's orientation factor $F(\theta)$ is related to the birefringence Δn by the following equation [19,20]:

$$F(\theta) = \langle P_2(\theta) \rangle = \frac{\Delta n}{\Delta n_{\max}} \tag{13}$$

where $\Delta n_{\max}$ is the intrinsic maximum birefringence, which corresponds to the case where all the molecules are perfectly aligned. If all polymer chains were aligned parallel to the fiber axis, the optical orientation factor $F(\theta)$ would be 1. For an isotropic system where there is no orientation $F(\theta)$ would be 0. The value of $\Delta n_{\max}$ for PP fiber is taken to be 0.045 [21]. Table 1 gives the variation of the orientation function with the draw ratio at different stretching speed. It is clear that, as the speed of stretching increases the orientation of the chains increases for the same draw ratio.

3.3. Effect of the stretching speed on transverse sectional area of PP fiber

When a fiber is deformed by an axial load, in addition to a change in length, a change in the cross-sectional area is produced. Experiments show that the Poisson ratio is a constant [22]. The decrease of the transverse sections of the fiber results from stretching the fibers is compensating the increase in the fiber length to keep Poisson's ratio constant during elastic deformation [22].

Fig. 8(a) shows the variation of the transverse sectional area of PP fibers with the draw ratio at the velocities 0.0596 and 12 cm/s, respectively. The used stepper motor, together with the mechanical parts, generates a fixed stretching force S. The force exerted by the motor was found $S = 50$ N (determined by force equilibrium method). While the breaking force of the fiber was found 0.4 N. Therefore, it was assumed that the fiber presented negligible resistance force against the machine force. Hence, the applied force to the fiber during stretching was considered constant. Accordingly the stretching stress $\sigma = S/A$ is inversely proportional to the fiber cross-section A. Fig. 8(b) shows the stress ($\sigma \propto 1/A$)–strain ε ($\varepsilon = \mathrm{DR}-1$) curves of PP fibers at different stretching speeds (different strain rates). From the figure it is clear that yield strength increases as the stretching speed increases [23]. The graph shows also that the yield strain constant by increasing the stretching speed.

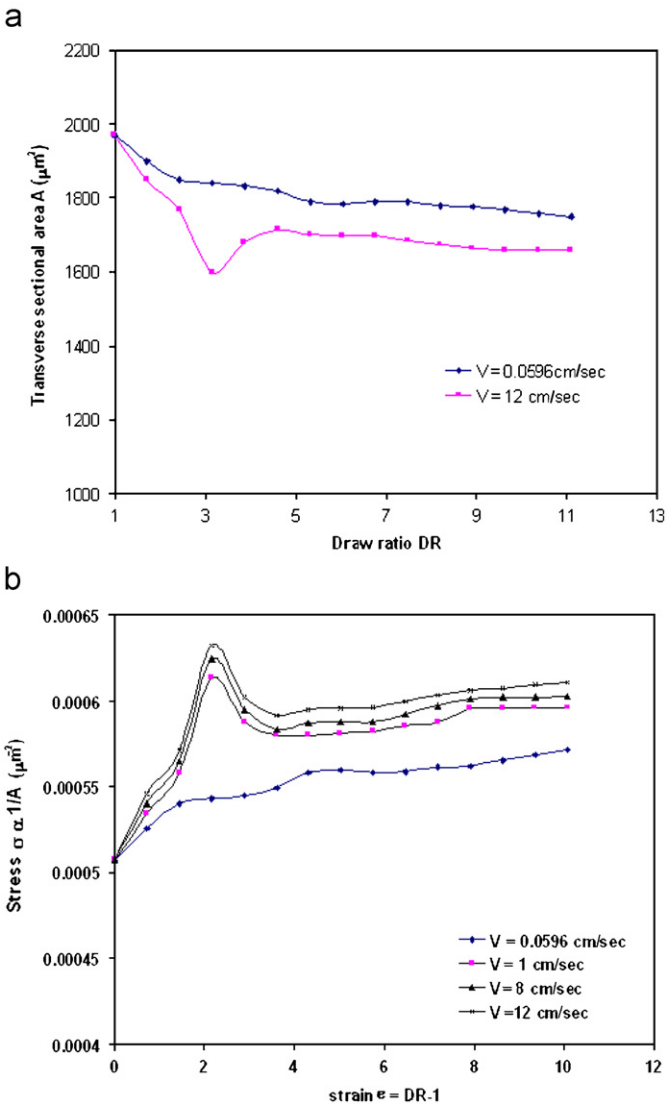

Fig. 8. Variation of the (a) transverse sectional area of PP fibers with the draw ratio at two different stretching speeds and (b) stress σ with the strain (ε) of PP fibers at different stretching speeds (different strain rates).

3.4. Suitable stretching speeds for PP fibers

Necking is a smoothed jump in cross-sectional area of long and thin bars propagating with a constant speed. This necking phenomenon usually occurs when a homogeneous solid polymeric bar (fiber or film) is stretched uniaxially [24,25]. In this case the polymer fiber is not deformed homogeneously. Instead, three almost uniform sections occur in the sample: two being nearly equal to its initial thickness. These sections are jointed by a relatively short transition necking zone (third uniform section) that propagates with a constant speed along the fiber as a stepwise wave in the direction of the fiber's thick end as clear in the first microinterferogram of Fig. 9. Many investigators studied

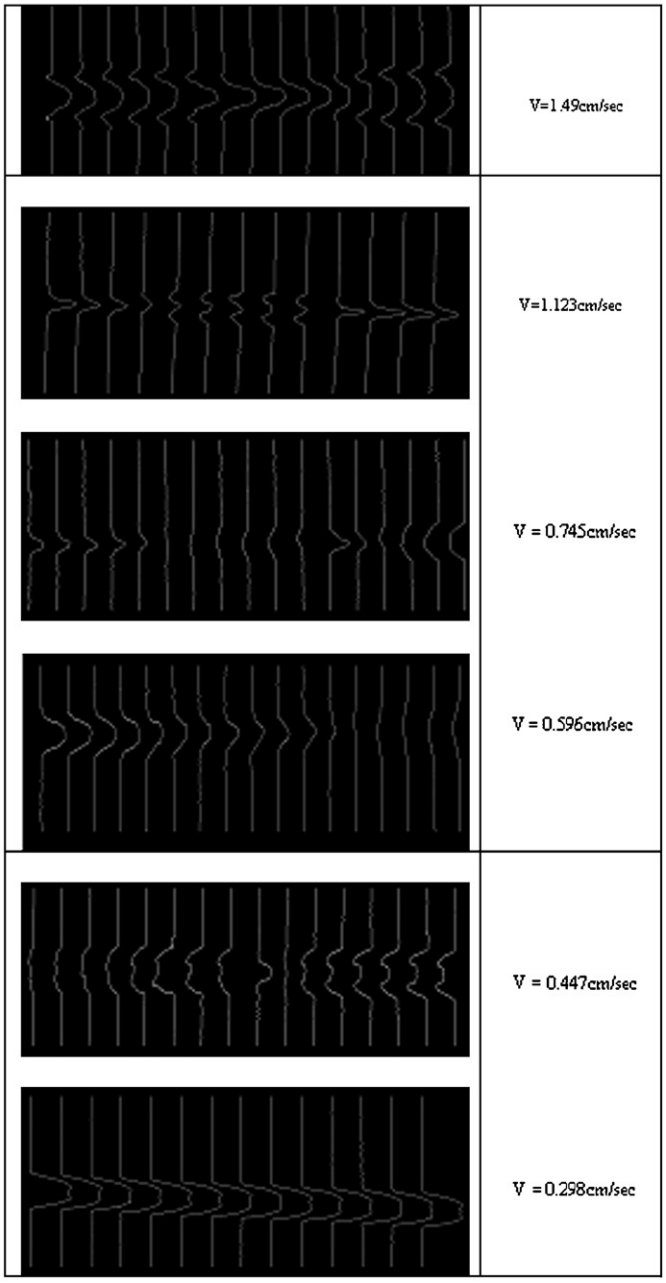

Fig. 9. Some of the obtained microinterferograms at different stretching speed. All of the stretching speed forming necking zones except at the threshold speed 0.298 cm/s at which we call threshold slow stretching.

the deformation of fibers at slow and fast stretching process without evaluating the limitations of slow and fast speed of stretching [10,26]. El-Dessouky [27] characterize the necking phenomena of PP fibers using Pluta polarizing interference microscope in case of offline drawing process.

Filaments of PP fibers are immersed in a suitable liquid with refractive index $n_L = 1.5068$. The speed of stretching is adjusted to be $V = 1.49$ cm/s, during this process necking deformation zones are formed as shown in Fig. 9. This process carried out at different velocities ranged from 0.298 to 1.49 cm/s. Fig. 9 shows some of the obtained microinterferograms at different speeds. These microinterferograms show necking formation at different speeds except at the threshold stretching speed $V_{th} = 0.298$ cm/s.

As the speed of stretching increases so the strain rate also increases. Strain rate has a complicated and dramatic effect on materials deformation processes because the energy expended during plastic deformation is largely dissipated as heat. The deformational work is nearly completely converted to heat, so the temperature of the sample is increased. At the small strain rate this heat generated is dissipated so quickly to the environment. But at high strain rate this part of the generated heat is dissipated to the environment and the other part is kept in the sample causing necking deformation [28,29].

In analogous to the well-known time–temperature superposition principle [30], one may establish a parallel principle for the draw ratio-stretching speed superposition. The obtained results as shown in Figs. 5–7, as well as in Table 1 (bold printed values) support this deduction. These results show that the physical state of a drawn fiber can be reached according to any of two distinct stretching regimes, either slow stretching to high draw ratio, or fast stretching to low draw ratio. The selection between these two stretching regimes depends on the specification requirements for the end use fiber. For example, the cross-section area of the end use fiber is an important parameter for many applications, if a strong thick fiber is required, hence undrawn fiber can be fast drawn to a low draw ratio, and vice versa.

It is recommended to stretch PP fibers slowly with low speed to avoid the occurrence of necking deformation, which occur during stretching with high speed (fast stretching). The speed that must be avoided is $V > 0.298$ cm/s.

4. Conclusion

A novel VOM device attached with multiple-beam interference system is designed. The advantage of this device is the determination of the refractive indices and birefringence of fibers simultaneously for each draw ratio during the online stretching process until breaking. From the above results we conclude that:

1. An empirical formula is suggested to correlate the change of birefringence of PP fibers and the speed of stretching. This formula indicates that the birefringence of PP fibers increase with increasing the speed of stretching.
2. The measured orientation function has high values, which indicates that the molecules constituting the fibers are highly oriented (more birefringent) during the stretching process and increases with increasing the speed of stretching.
3. The opto-mechanical device (VOM) may be used to measure pure mechanical parameters (yields strength, yields strain, breaking strength and strain at break) as well as the pure optical parameters.
4. The data obtained by the new opto-mechanical device supported the new mechanical concept draw ratio-stretching speed superposition.
5. The current study showed that it is possible to control both transverse-sectional area of the end use fiber and its mechanical strength simultaneously,
6. This device may be used for further studies of other mechanical relaxation phenomena online on the atomic level.

Acknowledgment

We would like to express our deep thanks to Prof. Dr. A.A. Hamza, for his useful discussions and lending many facilities.

References

[1] Flood JE, Nulf SA. Polym Eng Sci 1990;30:1504.
[2] Fujiyama M, Kitajima Y, Inata H. J Appl Polym Sci 2002;84:2128.

[3] Alberola N, Fugier M, Petit D, Fillon B. J Mater Sci 1995;30:860.
[4] Stefan R, Ludovic C, Helmut M, Johannes Klaus S. Rheol Acta 2002;41:332.
[5] Lia JX, Cheung WL, Chan CM. Polymer 1999;40:3641.
[6] Ohashi F, Hiroe T, Fujiwara K, Matsuo H. Polym Eng Sci 2002;42:1046.
[7] van der Wal A, Gaymans RJ. Polymer 1999;40:6045.
[8] Hamza AA, Sokkar TZN, El-Bakary MA. Meas Sci Technol 2004;15:831.
[9] Hamza AA, Sokkar TZN, El-Farahaty KA, EL-Dessouky HM. J Appl Polym Sci 2005;95:647.
[10] Hamza AA, Sokkar TZN, El-Farahaty KA, EL-Morsy MAM, EL-Dessouky HM. Opt Laser Technol 2005;37:532.
[11] Lee SY, Bassett DC, Olley RH. Polymer 2003;44:5961.
[12] Hearle JWS. J Appl Polym Sci 1963;7:1175.
[13] Barakat N, El-Hennawi HA. Text Res J 1971;41:391.
[14] Hamza AA, Sokkar TZN, Kabeel MA. J Phys D: Appl Phys 1985;18:1773.
[15] Hamza AA, Sokkar TZN, Mabrouk MA, El-Morsy MA. J Appl Polym 2000;77:3099.
[16] Ward IM. Proc Phys Soc 1962;80:1176.
[17] de Vries H. J Polym Sci 1979;XXXIV:761.
[18] Hamza AA, Kabeel MA. J Phys D: Appl Phys 1986;19:175.
[19] Hemsley DA. Applied polymer light microscopy. Amsterdam: Elsevier Science; 1989. 94p.
[20] Hermans PH. Contributions to the physics of cellulose fibers. Amsterdam: Elsevier; 1946. 159p.
[21] de Vries H. Colloid Polym Sci 1979:257.
[22] Sprackling MT. The mechanical properties of matter. Chatham: W & J Mackay & Co. Ltd.; 1970 chapter 1.
[23] Kuzyk Mark G. Polymer fiber optics. London: Taylor & Francis Group; 2007. p. 80.
[24] Leonov AI. J Rheol 1990;34:155.
[25] Kasei A, City N, Prefecture M. Lrish Scientist, Japan, 1999.
[26] Hamza AA, Sokkar TZN, Belal AE, EL-Dessouky HM, Yassien KM. Opt Laser Technol 2007;39:681.
[27] EL-Dessouky HM. J Appl Polym Sci 2007;105:757.
[28] Peterlin A. J Mater Sci 1971;6:490.
[29] Dasari A, Misra RDK. Mater Sci Technol 2002;18:1227.
[30] Shaw Montgomery T, Macknight Willim J. Introduction to polymer viscoelasticity. Hoboken, NJ: Wiley Interscience; 2005. p. 114.